Research Article | Vol. 25, No. 26 | 25 Dec 2017 | OPTICS EXPRESS 32401
Optics EXPRESS

Resonant mode conversions and Rabi oscillations in a fractional Schrödinger equation

YIQI ZHANG,[1,2,*] RONG WANG,[1] HUA ZHONG,[1] JINGWEN ZHANG,[1] MILIVOJ R. BELIĆ,[3,4] AND YANPENG ZHANG[1,5]

[1] *Key Laboratory for Physical Electronics and Devices of the Ministry of Education & Shaanxi Key Lab of Information Photonic Technique, Xi'an Jiaotong University, Xi'an 710049, China*
[2] *Department of Applied Physics, School of Science, Xi'an Jiaotong University, Xi'an 710049, China*
[3] *Science Program, Texas A&M University at Qatar, P.O. Box 23874, Doha, Qatar*
[4] *milivoj.belic@qatar.tamu.edu*
[5] *ypzhang@mail.xjtu.edu.cn*
[*] *zhangyiqi@mail.xjtu.edu.cn*

Abstract: In a theoretical and numerical analysis, we report resonant mode conversions and Rabi oscillations in the fractional Schrödinger equation through the longitudinal modulation of the transverse potential. As specific systems of interest, we select eigenmodes of the transverse Gaussian and periodic potentials. In the Gaussian potential, we find that an increasing number of eigenmodes can be supported as the Lévy index α is reduced from 2 to 1, and that the conversion distance between the first and third eigenmodes first decreases and then increases. In the periodic potential, we obtain a cascade conversion between the neighboring eigenmodes because the parity of eigenmodes remains the same. We also find that the conversion distances between the first and second eigenmodes, as well as between the second and third eigenmodes, decrease monotonously, while that between the first and third eigenmodes first decreases and then increases with increasing α. In addition, we find that for a certain α, these conversion distances can be equal to each other.

OCIS codes: (260.2710) Inhomogeneous optical media; (230.7370) Waveguides; (130.5296) Photonic crystal waveguides; (350.5500) Propagation; (160.1245) Artificially engineered materials.

References and links

1. F. Bloch, "Über die Quantenmechanik der Elektronen in Kristallgittern," Z. Phys. **52**, 555–600 (1929).
2. I. I. Rabi, "On the process of space quantization," Phys. Rev. **49**, 324–328 (1936).
3. F. Lederer, G. I. Stegeman, D. N. Christodoulides, G. Assanto, M. Segev, and Y. Silberberg, "Discrete solitons in optics," Phys. Rep. **463**, 1–126 (2008).
4. S. Longhi, "Quantum-optical analogies using photonic structures," Laser Photon. Rev. **3**, 243–261 (2009).
5. Y. V. Kartashov, B. A. Malomed, and L. Torner, "Solitons in nonlinear lattices," Rev. Mod. Phys. **83**, 247–305 (2011).
6. I. L. Garanovich, S. Longhi, A. A. Sukhorukov, and Y. S. Kivshar, "Light propagation and localization in modulated photonic lattices and waveguides," Phys. Rep. **518**, 1–79 (2012).
7. Y. V. Kartashov, V. V. Konotop, D. A. Zezyulin, and L. Torner, "Bloch oscillations in optical and Zeeman lattices in the presence of spin-orbit coupling," Phys. Rev. Lett. **117**, 215301 (2016).
8. Y. Q. Zhang, D. Zhang, Z. Y. Zhang, C. B. Li, Y. P. Zhang, F. L. Li, M. R. Belić, and M. Xiao, "Optical Bloch oscillation and Zener tunneling in an atomic system," Optica **4**, 571–575 (2017).
9. K. O. Hill, B. Malo, K. A. Vineberg, F. Bilodeau, D. C. Johnson, and I. Skinner, "Efficient mode conversion in telecommunication fibre using externally written gratings," Electronics Letters **26**, 1270–1272 (1990).
10. K. S. Lee and T. Erdogan, "Fiber mode coupling in transmissive and reflective tilted fiber gratings," Appl. Opt. **39**, 1394–1404 (2000).
11. Y. V. Kartashov, V. A. Vysloukh, and L. Torner, "Resonant mode oscillations in modulated waveguiding structures," Phys. Rev. Lett. **99**, 233903 (2007).
12. V. A. Vysloukh, Y. V. Kartashov, and K. Staliunas, "Efficient mode conversion in guiding structures with longitudinal modulation of nonlinearity," Opt. Lett. **40**, 4631–4634 (2015).
13. X. Zhang, F. Ye, Y. V. Kartashov, and X. Chen, "Rabi oscillations and stimulated mode conversion on the subwavelength scale," Opt. Express **23**, 6731–6737 (2015).
14. M. Ornigotti, G. D. Valle, T. T. Fernandez, A. Coppa, V. Foglietti, P. Laporta, and S. Longhi, "Visualization of two-photon Rabi oscillations in evanescently coupled optical waveguides," J. Phys. B: At., Mol. Opt. Phys. **41**,

#310224 https://doi.org/10.1364/OE.25.032401
Journal © 2017 Received 30 Oct 2017; revised 4 Dec 2017; accepted 5 Dec 2017; published 12 Dec 2017

Optics EXPRESS

085402 (2008).
15. K. G. Makris, D. N. Christodoulides, O. Peleg, M. Segev, and D. Kip, "Optical transitions and Rabi oscillations in waveguide arrays," Opt. Express **16**, 10309–10314 (2008).
16. K. Shandarova, C. E. Rüter, D. Kip, K. G. Makris, D. N. Christodoulides, O. Peleg, and M. Segev, "Experimental observation of Rabi oscillations in photonic lattices," Phys. Rev. Lett. **102**, 123905 (2009).
17. V. A. Vysloukh and Y. V. Kartashov, "Resonant mode conversion in the waveguides with unbroken and broken PT symmetry," Opt. Lett. **39**, 5933–5936 (2014).
18. G. K. L. Wong, M. S. Kang, H. W. Lee, F. Biancalana, C. Conti, T. Weiss, and P. S. J. Russell, "Excitation of orbital angular momentum resonances in helically twisted photonic crystal fiber," Science **337**, 446–449 (2012).
19. Y. V. Kartashov, V. A. Vysloukh, and L. Torner, "Dynamics of topological light states in spiraling structures," Opt. Lett. **38**, 3414–3417 (2013).
20. Y. V. Kartashov, A. Szameit, V. A. Vysloukh, and L. Torner, "Light tunneling inhibition and anisotropic diffraction engineering in two-dimensional waveguide arrays," Opt. Lett. **34**, 2906–2908 (2009).
21. Y. V. Kartashov, V. A. Vysloukh, and L. Torner, "Enhancement and inhibition of light tunneling mediated by resonant mode conversion," Opt. Lett. **39**, 933–936 (2014).
22. Z. Yu and S. Fan, "Complete optical isolation created by indirect interband photonic transitions," Nat. Photon. **3**, 91–94 (2009).
23. N. Laskin, "Fractional quantum mechanics and Lévy path integrals," Phys. Lett. A **268**, 298–305 (2000).
24. N. Laskin, "Fractional quantum mechanics," Phys. Rev. E **62**, 3135–3145 (2000).
25. N. Laskin, "Fractional Schrödinger equation," Phys. Rev. E **66**, 056108 (2002).
26. Y. Q. Zhang, X. Liu, M. R. Belić, W. P. Zhong, Y. P. Zhang, and M. Xiao, "Propagation dynamics of a light beam in a fractional Schrödinger equation," Phys. Rev. Lett. **115**, 180403 (2015).
27. Y. Q. Zhang, H. Zhong, M. R. Belić, N. Ahmed, Y. P. Zhang, and M. Xiao, "Diffraction-free beams in fractional Schrödinger equation," Sci. Rep. **6**, 23645 (2016).
28. Y. Q. Zhang, H. Zhong, M. R. Belić, Y. Zhu, W. P. Zhong, Y. P. Zhang, D. N. Christodoulides, and M. Xiao, "Pt symmetry in a fractional Schrödinger equation," Laser Photon. Rev. **10**, 526–531 (2016).
29. A. Liemert and A. Kienle, "Fractional Schrödinger equation in the presence of the linear potential," Mathematics **4**, 31 (2016).
30. C. Huang and L. Dong, "Beam propagation management in a fractional Schrödinger equation," Sci. Rep. **7**, 5442 (2017).
31. B. Guo and D. Huang, "Existence and stability of standing waves for nonlinear fractional Schrödinger equations," J. Math. Phys. **53**, 083702 (2012).
32. C. Klein, C. Sparber, and P. Markowich, "Numerical study of fractional nonlinear Schrödinger equations," Proc. R.Soc. A **470**, 20140364 (2014).
33. L. Zhang, C. Li, H. Zhong, C. Xu, D. Lei, Y. Li, and D. Fan, "Propagation dynamics of super-Gaussian beams in fractional Schrödinger equation: from linear to nonlinear regimes," Opt. Express **24**, 14406–14418 (2016).
34. C. Huang and L. Dong, "Gap solitons in the nonlinear fractional Schrödinger equation with an optical lattice," Opt. Lett. **41**, 5636–5639 (2016).
35. S. Longhi, "Fractional Schrödinger equation in optics," Opt. Lett. **40**, 1117–1120 (2015).
36. D. Zhang, Y. Q. Zhang, Z. Y. Zhang, N. Ahmed, Y. P. Zhang, F. L. Li, M. R. Belić, and M. Xiao, "Unveiling the link between fractional Schrödinger equation and light propagation in honeycomb lattice," Ann. Phys. (Berlin) **529**, 1700149 (2017).

1. Introduction

Similar to Bloch oscillations [1], Rabi oscillations [2] were first predicated in quantum mechanics and then much later demonstrated experimentally. Different from Bloch oscillations, which are intra-band oscillations that require a dc field to be applied to a periodic potential, Rabi oscillations are inter-band oscillations that require only an ac field to be applied. Nowadays, both types of oscillations are frequently reported in optics, for example Bloch in various systems [3–8], and Rabi in more specific systems: fibers [9, 10], multimode waveguides [11–13], coupled waveguides [14], waveguide arrays [15–17], and two-dimensional structures [18, 19]. In optics, the longitudinal periodic modulation of the refractive index change plays the role of an ac field in quantum systems, and the Rabi oscillations are indicated by the resonant mode conversions. It has been demonstrated that the longitudinal modulation can help in inhibiting light tunneling [20, 21] and realizing optical isolation [22].

Until now, research progress has been achieved in both paraxial and nonparaxial guiding structures. To the best of our knowledge, resonant mode conversions and Rabi oscillations in the fractional Schrödinger equation (FSE) have not been reported yet. The FSE is the fundamental

Optics EXPRESS

equation of the fractional quantum mechanics [23–25]. It features the fractional Laplacian operator instead of the regular one. The substitution of the regular, integer-dimensional Laplacian by a fraction-dimensional one, brings a profound change in the behavior of the wave function. In optics, the fractional Laplacian causes non-parabolic dispersion, which suggests the possibility of directly modulating the dispersion of a physical system. The problem is – the dearth of real physical systems described by the FSE. Nonetheless, some interesting phenomena based on FSE were reported recently [26–30], and even some nonlinear aspects were addressed [31–34]. As it happens in linear optics, many optical processes are made more manageable by utilizing the Fourier transform; this holds for the fractional Laplacian operation in FSE as well [35]. Very recently, a potential link between the FSE and the beam propagation in honeycomb lattice was established, based on the Dirac-Weyl equation [36]. This also represented an attempt to identify a real physical system that can be described by the FSE.

The aim of the present paper is to investigate resonant mode conversions and Rabi oscillations in FSE, by considering two kinds of potentials: Gaussian and periodic potentials. The influence of the fractional Laplacian on phenomena coming from the two potentials will be discussed in some detail. The organization of the paper is as follows. In Sec. 2, we provide a brief theoretical introduction and the method of analysis applied to the system, including how to find the period of Rabi oscillation. In Sec. 3, we present results coming from the numerical simulation and the corresponding discussion in detail. We divide this section into two subsections, each focusing separately on the Gaussian potential and on the periodic potential. We conclude the paper in Sec. 4.

2. Theoretical modeling

The fractional Schrödinger equation with a longitudinally-modulated potential can be written as

$$i\frac{\partial\psi}{\partial z} = \frac{1}{2}\left(-\frac{\partial^2}{\partial x^2}\right)^{\alpha/2}\psi + pR(x)[1+\mu\cos(\Omega_z z)]\psi, \tag{1}$$

in which $1 < \alpha \leq 2$ is the Lévy index, $R(x)$ describes the profile of the transverse potential, p determines the depth of the potential, Ω_z is the longitudinal modulation frequency, and $\mu < 1$ is the strength of the longitudinal modulation.

We seek the stationary solution of Eq. (1) when $\mu = 0$, with an ansatz

$$\psi(x,z) = \phi(x)\exp(i\beta z). \tag{2}$$

Plugging this into Eq. (1), one obtains the linear eigenvalue problem

$$-\beta\phi = \frac{1}{2}\left(-\frac{\partial^2}{\partial x^2}\right)^{\alpha/2}\phi + pR(x)\phi. \tag{3}$$

According to the Floquet-Bloch theorem, $\phi(x)$ can be written as $\phi(x) = w_k(x)\exp(ikx)$, where $w_k(x) = w_k(x+d_0)$ is spatially periodic and d_0 is the period. One can expand $w_k(x)$ and the potential in a series of plane-waves, $w_k(x) = \sum_n c_n \exp(iK_n x)$, with $K_n = 2\pi n/d_0$ and $V(x) = pR(x) = \sum_m P_m \exp(iK_m x)$, where

$$P_m = \frac{1}{d_0}\int_{d_0} V(x)\exp(-iK_m x)dx.$$

Inserting these series into Eq. (3), one obtains

$$\sum_n \left[\beta + \frac{1}{2}|k+K_n|^\alpha\right] c_n \exp[i(k+K_n)x] + \sum_{m,n} P_m c_n \exp[i(k+K_n+K_m)x] = 0. \tag{4}$$

Optics EXPRESS

Multiplying the above equation by $\exp[-i(k+K_q)x]$ and integrating over $x \in (-\infty, +\infty)$, one ends up with

$$-\frac{1}{2}|k+K_q|^{\alpha}c_q - \sum_m P_m c_{q-m} = \beta c_q, \tag{5}$$

which is Eq. (3) in the discrete form, with c_n being the eigenvector components. We should note that Eqs. (4) and (5) are feasible not only for periodic potentials, but also for non-periodic potentials.

For the sake of investigating the mode conversion, we adopt the superposition of two eigenmodes $\phi_{m,n}$ as an input

$$\psi(x,z) = C_m(z)\phi_m(x)\exp(i\beta_m z) + C_n(z)\phi_n(x)\exp(i\beta_n z), \tag{6}$$

where $C_{m,n}$ are complex weight coefficients and $\Omega_z = \beta_m - \beta_n$. Combining Eqs. (1), (3) and (6), and after some algebra, one obtains the coupled set of equations

$$\begin{aligned} i\frac{\partial C_m}{\partial z} &= -\frac{1}{2}p\mu\frac{\langle\phi_m R\phi_n\rangle}{\langle\phi_m\phi_m\rangle}C_n, \\ i\frac{\partial C_n}{\partial z} &= -\frac{1}{2}p\mu\frac{\langle\phi_n R\phi_m\rangle}{\langle\phi_n\phi_n\rangle}C_m, \end{aligned} \tag{7}$$

where $\langle\phi_m R\phi_n\rangle = \int_{-\infty}^{+\infty}\phi_m^*(x)R(x)\phi_n(x)dx$, with the asterisk representing the conjugate operation. Based on Eq. (7), the mode conversion period can be obtained, as

$$z_{\mathrm{crmn}} = \frac{\pi}{|\Omega_x|}, \tag{8}$$

with

$$\Omega_x = \frac{\mu p}{2}\cdot\frac{\langle\phi_m R\phi_n\rangle}{\sqrt{\langle\phi_m\phi_m\rangle\langle\phi_n\phi_n\rangle}}.$$

We note that the mode conversion happens at half the period, i.e., at $z_{\mathrm{crmn}}/2$. As previously noted [11], mode conversion only happens between the modes with identical parity, because the oscillation frequency Ω_x will be 0, due to $\langle\phi_m R\phi_n\rangle = 0$.

3. Results and discussion

3.1. Gaussian transverse potential

We begin with a Gaussian transverse potential of the form $R(x) = \exp[-(x/W)^2]$, and choose $p = 2.3$ and $W = 2$. The eigenmodes of the potential are displayed in Fig. 1. First of all, one finds that the energy level of the first eigenmode does not change, while those of other eigenmodes increase in the fractional Schrödinger equation. Secondly, the width of the eigenmode decreases gradually with decreasing the Lévy index α. In addition, higher-order eigenmodes appear gradually in the same Gaussian potential for the FSE. One finds that the potential supports 4 eigenmodes with $\alpha = 1.5$ [Fig. 1(b)], and 5 eigenmodes with $\alpha = 1$ [Fig. 1(c)].

To see mode conversion, we set the third eigenmode as the input, with $\Omega_z = \beta_1 - \beta_3$ and $\mu = 0.1$; the propagation for different α is shown in Figs. 1(d)-1(f). One indeed observes the Rabi oscillation that indicates the mode conversion during propagation. In Fig. 1(d), the propagation is damped during propagation, due to the radiation, however the radiation is much suppressed when α decreases, as shown in Figs. 1(e) and 1(f).

Since the Gaussian potential supports 5 eigenmodes in the FSE with $\alpha = 1$, we also investigate the mode conversion among the first, third and fifth modes. We utilize the fifth mode as the input

Optics EXPRESS

and set the longitudinal modulation frequency to be $\Omega_z = \beta_3 - \beta_5$ at the very beginning. When the propagation distance is bigger than $z_{\mathrm{cr35}}/2$ [viz. $m = 3$ and $n = 5$ in Eq. (8)], where the fifth mode has already conversed into the third mode, we change $\Omega_z = \beta_3 - \beta_5$ into $\Omega_z = \beta_1 - \beta_3$. After a further propagation for distance z_{cr13}, which is the Rabi oscillation period between the first and third modes, we change Ω_z back into $\Omega_z = \beta_3 - \beta_5$. Finally, we recover the fifth mode at the output place $z = z_{\mathrm{cr13}} + z_{\mathrm{cr35}}$. The whole propagation that illustrates the cascade conversion is displayed in Fig. 1(g).

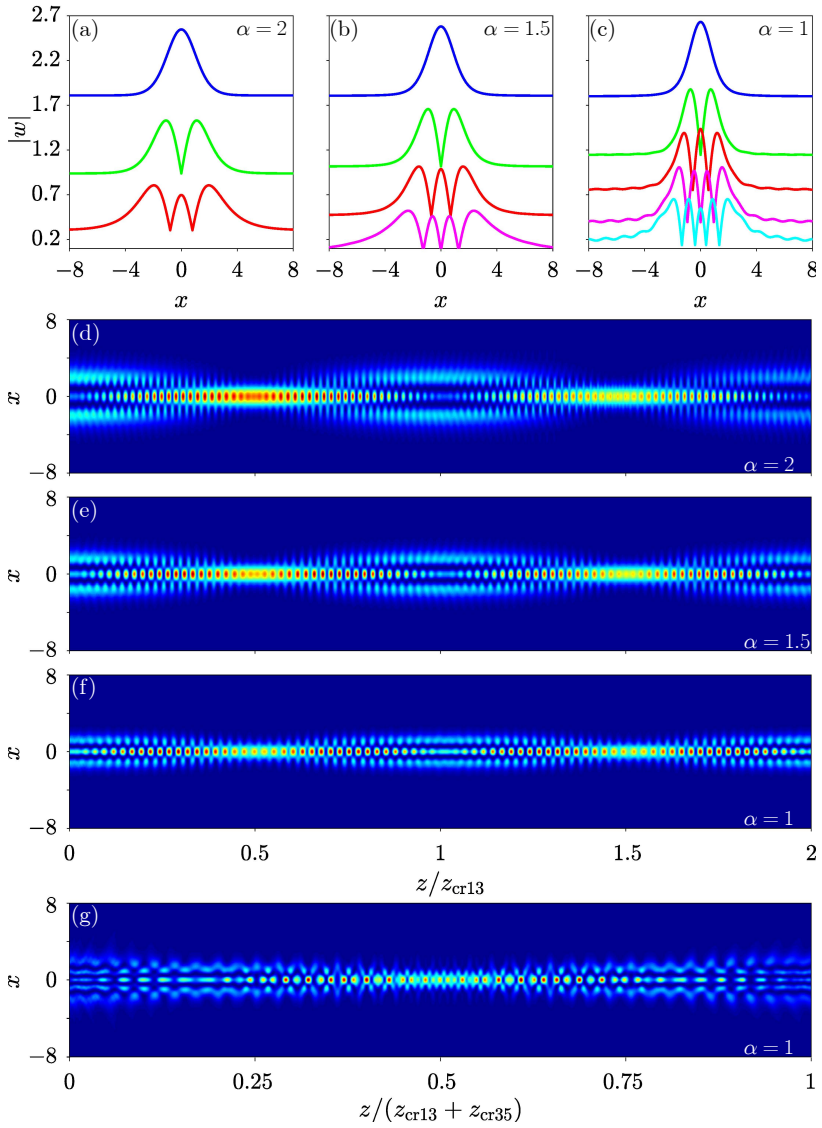

Fig. 1. (a)-(c) Eigenmodes of the Gaussian potential, corresponding to $\alpha = 2$, 1.5 and 1, respectively. The blue, green, red, magenta, and cyan curves indicate the first, second, third, fourth, and fifth modes, respectively. All the modes are shifted vertically, to show the corresponding energy levels in the potential. (d)-(f) Resonant mode conversions between the first and third modes, corresponding to $\alpha = 2$, 1.5 and 1, respectively. (g) Resonant mode conversion among the first, third and fifth modes, corresponding to $\alpha = 1$.

Optics EXPRESS

It is worth mentioning that the longitudinal frequency $\Omega_z = \beta_m - \beta_n$ is the resonant frequency for the mode conversion between the m^{th} and n^{th} eigenmodes. Normally, the efficiency of mode conversion is the highest at the resonant longitudinal frequency. When there is an additional detuning δ from this resonant frequency, e.g., $\Omega_z = \beta_m - \beta_n + \delta$, the efficiency of the mode conversion will be affected. Numerical simulations demonstrate that the longer the conversion period, the higher the efficiency of the mode conversion. In Figs. 2(a)-2(c), we show the relation between the conversion period z_{cr} and the detuning δ. Regardless of the value of Lévy index α, the conversion distance (i.e., the corresponding efficiency of the mode conversion) is indeed the highest at $\delta = 0$, i.e., at the resonant frequency. However, the efficiency drops sharply when there is a detuning from the resonant frequency. According to Figs. 2(a)-2(c), one may find that the conversion distance at the resonant frequency decreases first [Fig. 2(b)] and then increases [Fig. 2(c)] with decreasing Lévy index α. To show this phenomenon more clearly, we present the analytical relation [Eq. (8)] between the conversion period z_{cr13} and the Lévy index α by choosing certain values for the longitudinal modulation depth μ [Fig. 2(d)]. The analytical results verified the numerical findings, and the minimum conversion distance happens at $\alpha \sim 1.6241$. We exhibit the relation between the conversion period z_{cr13} and the longitudinal modulation depth μ in Fig. 2(e). One observes that the effect on the conversion period z_{cr13} coming from the Lévy index α becomes small with increasing μ.

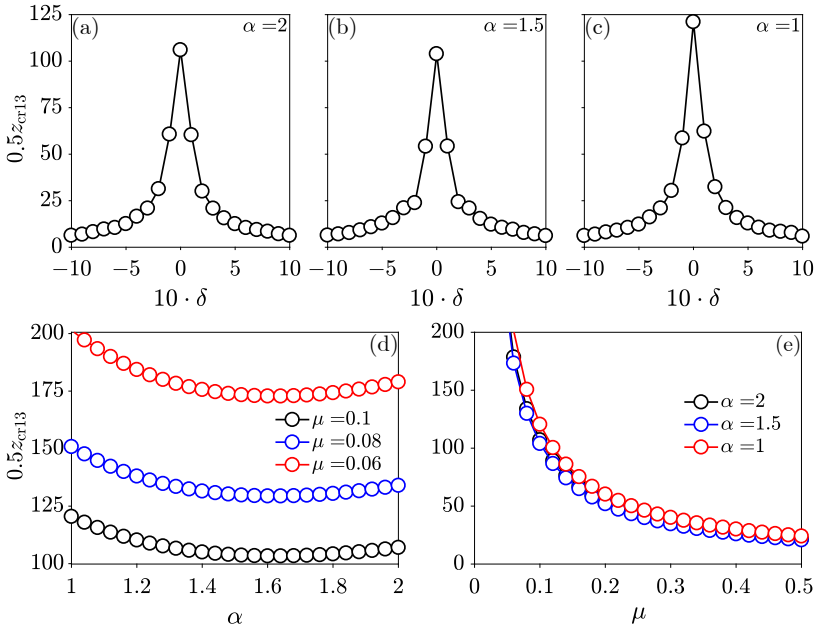

Fig. 2. (a)-(c) Relation between the conversion period z_{cr13} and the detuning δ, corresponding to $\alpha = 2$, 1.5 and 1, respectively. (d) Relation between the conversion period $z_{\text{cr13}}/2$ and the Lévy index α at different longitudinal modulation depths μ. (e) Relation between the conversion period z_{cr13} and the longitudinal modulation depth μ, for different Lévy indices α.

3.2. *Periodic transverse potential*

For the periodic transverse potential, we choose $p = 1$ and $R(x) = \cos(2\pi x/d_0)$, with $d_0 = 2$. According to Eq. (5), the band structure of this potential corresponding to different Lévy indices α can be easily obtained. We choose $\alpha = 2$, 1.5 and 1 as examples, and the corresponding band structures (only the first three bands) are displayed in Figs. 3(a)-3(c). The first three eigenmodes

Optics EXPRESS

at $k_x = 0.55$ [indicated by the black, blue and red dots in Figs. 3(a)-3(c)] are shown in Figs. 3(d)-3(f). In the fractional Schrödinger equation, the width of the bands are much narrower and the bands (except the first one) move upward along the β axis, in comparison with those of the regular Schrödinger equation [Fig. 3(a)]. Also, the parabolic profile of the first band becomes symmetrically linear with decreasing Lévy index α [see the band around the boundary of the first Brillouin zone in Fig. 3(c)].

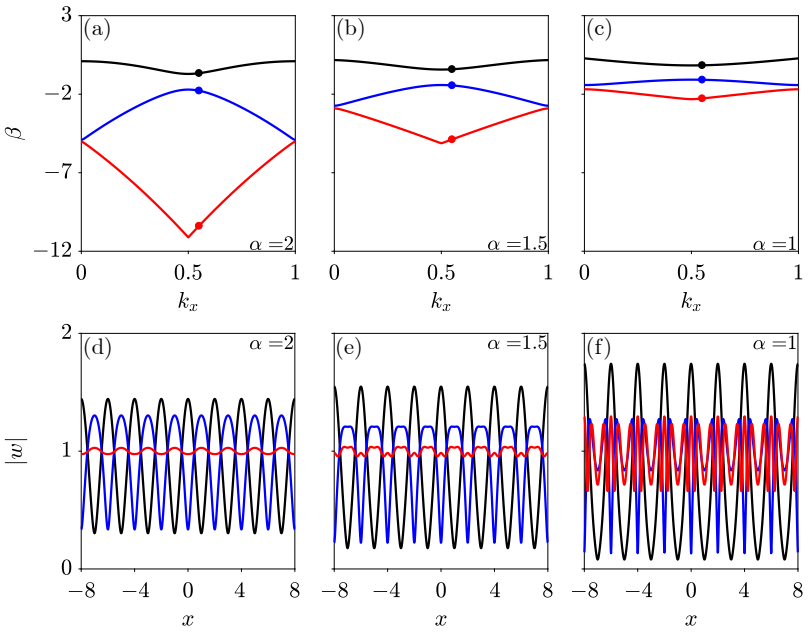

Fig. 3. (a)-(c) Band structure in the first Brillouin zone, corresponding to $\alpha = 2$, 1.5 and 1, respectively. The black, blue and red curves represent the first, second and third bands. (d)-(f) Eigenmodes corresponding to $\alpha = 2$, 1.5 and 1, respectively. The black, blue and red modes are corresponding to the black, blue and red dots ($k_x = 0.55$) in the band structure.

As concerns the eigenmodes in Figs. 3(d)-3(f), one finds that the width of the eigenmodes increases with decreasing Lévy index α. Although the first eigenmode is always cosine-like, which reflects the profile of the periodic potential, the profiles of other eigenmodes vary greatly with the Lévy index α; a dip appears gradually in the wave crest of the second as well as of the third eigenmode, and a peak appears gradually in the wave valley of the third eigenmode. Different from the eigenmodes of the Gaussian potential displayed in Fig. 1, the parities of eigenmonds here are always equal. Therefore, the conversion between the neighboring eigenmodes [viz. the n^{th} and $(n+1)^{\text{th}}$ eigenmodes] is possible.

In Fig. 4, we show the cascading mode conversion among the first, second and third eigenmodes, when the first eigenmode is the input $\psi(z=0) = \phi_1(x)\exp(ik_x x)$. The process is quite similar to that in Fig. 1(g): we set the longitudinal frequency $\Omega_z = \beta_1 - \beta_2$ in the propagation distance $z \le z_{\text{cr12}}/2$, where the first eigenmode converses into the second eigenmode, and then let $\Omega_z = \beta_2 - \beta_3$ in the next propagation distance $z_{\text{cr12}}/2 < z \le z_{\text{cr23}}/2$. To better observe the mode conversion, we also introduce the weight of the eigenmode during propagation $c_{\text{eff}} = \langle \phi_n \psi(z)\exp(-ik_x x)\rangle$, in which the integral is over one period $-d_0/2 \le x \le d_0/2$. In Figs. 4(a), 4(c) and 4(e), we show the cascade mode conversion, while in Figs. 4(b), 4(d) and 4(f), we present the weight of each eigenmode during propagation (the black, blue and red curves are for the first, second and third eigenmodes, respectively). No doubt, one observes a perfect mode conversion in the periodic potential, no matter what the value of α is. One may also notice

Optics EXPRESS

that the conversion period z_{cr12} between the first and the second eigenmode is larger than that between the second and the third eigenmode z_{cr23}. However, one cannot recognize the changing trend of the conversion distance with α between different eigenmodes, in Fig. 4. As a result, we show the relation between the conversion distance and α in Fig. 5(a). The conversion period z_{cr12} between the first and second eigenmodes (blue curve, left y axis) decreases monotonously with increasing α, while the conversion period z_{cr23} between the second and third eigenmodes (red solid curve, right y axis) decreases first and then increases with increasing α. Numerical results demonstrate that the minimum conversion distance corresponds to $\alpha \sim 1.297$.

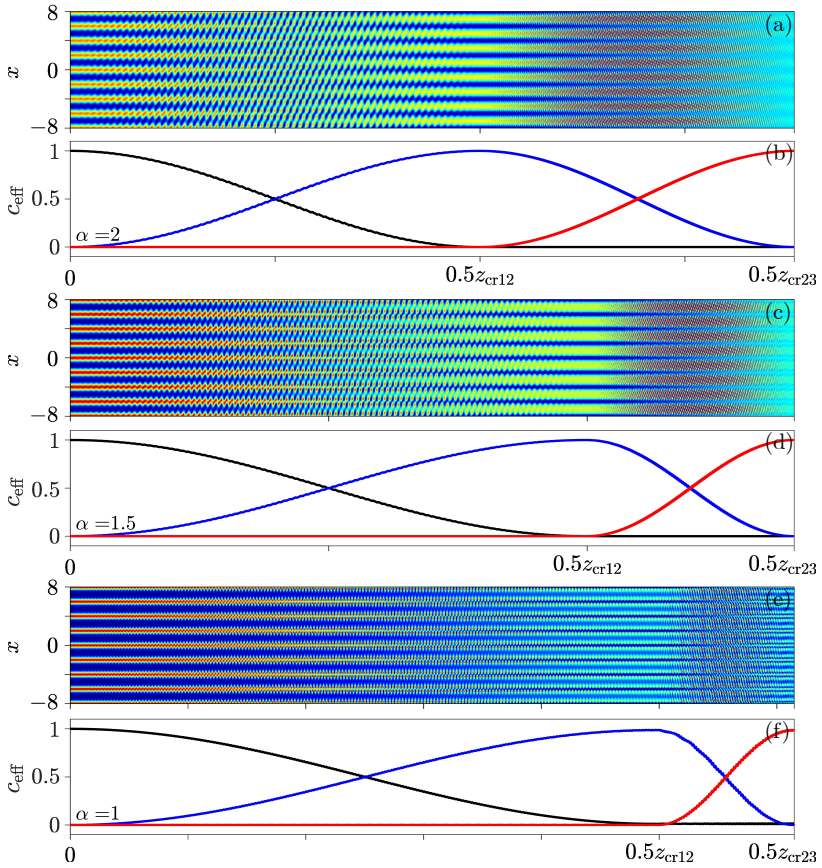

Fig. 4. (a) Cascading mode conversion at $\alpha = 2$. (b) Weight of the eigenmode during propagation. (c)&(d) and (e)&(f) are same as (a)&(b), but for $\alpha = 1.5$ and $\alpha = 1$, respectively. Black, blue and red curves in (b), (d) and (f) represent the weights of the first, second and third eigenmodes, respectively. The other parameter: $\mu = 0.04$.

Similar to the mode conversion in the Gaussian potential, the first and the third eigenmode can also converse into each other. In Figs. 5(b)-5(d), we present the mode conversions that accompany Rabi oscillations. The conversion distance for this case is also displayed in Fig. 5(a), the red dashed curve. Clearly, the conversion distance decreases monotonically with the increasing α, which is different from the case of the Gaussian potential, as shown in Fig. 2(d).

It is also interesting to find that the red curves touch each other at $\alpha_t \sim 1.242$ in Fig. 5(a), which means that the conversion distance between the first and third eigenmodes z_{cr13} almost equals that between the second and third eigenmodes z_{cr23}. The reason is that the coupling coefficients are almost the same for this Lévy index. That is, according to Eq. (8), $\langle \phi_1^* R \phi_3 \rangle \approx \langle \phi_2^* R \phi_3 \rangle$. In

Optics EXPRESS

Fig. 5(e), the first three eigenmodes at this point are exhibited; the profiles of the second and the third eigenmodes, located in the notches of the first eigenmode, are quite similar, except in the regions around the peaks of the first eigenmode. We note that the touching point α_t between z_{cr13} and z_{cr23} will not be affected by the longitudinal modulation strenghth μ.

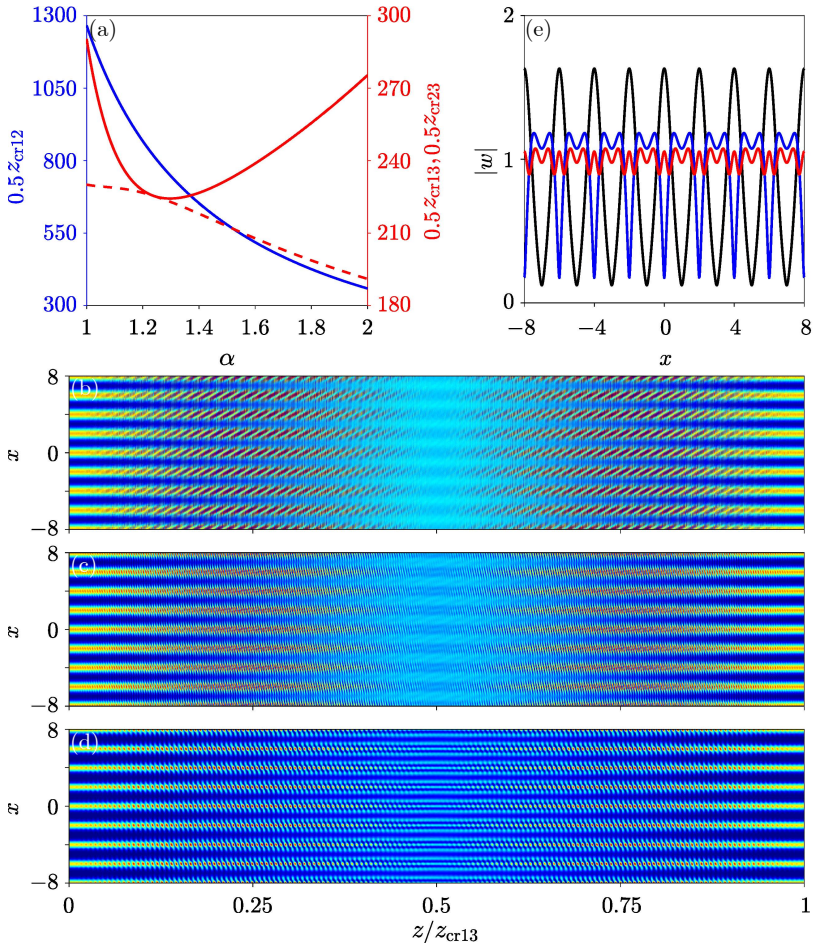

Fig. 5. (a) Conversion distance between different modes. (b) Weight of the eigenmode during propagation. The blue curve refers to the left y axis, while the red curves (solid and dashed curves are z_{cr23} and z_{cr13}, respectively) refer to the right y axis. (b)-(d) Mode conversion between the first and third eigenmodes with $\alpha = 2$, 1.5 and 1, respectively. (e) Eigenmodes at $\alpha \approx 1.242$. The setup is as in Fig. 3(b). The other parameter: $\mu = 0.04$.

4. Conclusion

In summary, we have investigated resonant mode conversions and Rabi oscillations in the fractional Schrödinger equation, through the longitudinal modulation of the transverse Gaussian and periodic potentials. We find that the oscillation period and the conversion efficiency can be effectively manipulated by the Lévy index. This research provides a potential new avenue for the control of light in propagation.

Optics EXPRESS

Funding

National Key R&D Program of China (2017YFA0303700); Natural Science Foundation of Shaanxi Province (2017JZ019); China Postdoctoral Science Foundation (2016M600777); National Natural Science Foundation of China (11474228); Qatar National Research Fund (NPRP 8-028-1-001).

Acknowledgments

MRB acknowledges support by the Al Sraiya Holding Group.